

1 Regional benthic $\delta^{18}\text{O}$ stacks for the “41-kyr world” - an Atlantic-Pacific divergence 2 between 1.8-1.9 Ma 3

4 Yuxin Zhou¹, Lorraine E. Lisiecki¹, Taehee Lee², Geoffrey Gebbie³, and Charles Lawrence²

5 ¹Department of Earth Science, University of California, Santa Barbara.

6 ²Division of Applied Mathematics, Brown University.

7 ³Physical Oceanography Department, Woods Hole Oceanographic Institution.

8 Corresponding author: Yuxin Zhou (yuxin_zhou@ucsb.edu)
9

10 Key points

- 11 • New Atlantic and Pacific benthic $\delta^{18}\text{O}$ stacks show different patterns between 1.8-1.9 Ma.
- 12 • The Atlantic-Pacific difference in this portion of the 41-kyr world may be caused by
13 regional sensitivity to relatively strong precession.
- 14 • Regional benthic $\delta^{18}\text{O}$ stacks are preferable to global stacks for stratigraphic alignment.
15

16 Abstract

17 Benthic $\delta^{18}\text{O}$ stacks are the benchmarks by which paleoceanographic data are stratigraphically
18 aligned and compared. However, a recent study found that between 1.8-1.9 million years ago
19 (Ma) several Ceara Rise records differed substantially from the widely used LR04 global stack.
20 Here, we use new Bayesian stacking software to construct regional stacks and demonstrate a
21 geographical divergence in benthic $\delta^{18}\text{O}$ features from 1.8-1.9 Ma. The pattern of isotopic stage
22 features observed in the Ceara Rise is widespread throughout the Atlantic and differs notably
23 from Pacific records. We propose that this regional difference in isotopic stages may be the result
24 of relatively strong precession forcing and weaker obliquity forcing between 1.8-1.9 Ma. In
25 accordance with the Antiphase Hypothesis, our results highlight a period of apparent sensitivity
26 to regional precession forcing that is masked during most of the 41-kyr world due to the
27 amplitude modulation of obliquity forcing.
28

29 Plain language summary

30 To determine the age of deep-sea sediments, often the oxygen isotope ratios of microfossils are
31 measured and compared to a previously compiled global benchmark. Recently, one of the most
32 widely used oxygen isotope benchmarks has been challenged based on a comparison with
33 several Atlantic records. In this study we assess several lines of evidence including utilizing
34 newly available data and software. We confirm the challenge to the global oxygen isotope
35 benchmark and find that it is more widespread than originally realized. Particularly, we find that
36 oxygen isotope records display different patterns between the Atlantic and Pacific Oceans from
37 1.8-1.9 million years ago (Ma). We propose that this difference is the result of the opposing
38 seasonal solar radiation anomalies received by the northern and southern hemispheres, which
39 exhibited particularly large amplitudes during this time. Our study adds supporting evidence to a
40 hypothesis that explains the dominant frequency of climatic cycles from 1.2-2.6 Ma.
41

42 Introduction

43 Benthic $\delta^{18}\text{O}$ stacks set benchmarks for comparison of paleoceanographic data (e.g., Ahn et al.,
44 2017; Lisiecki & Raymo, 2005; Martinson et al., 1987) and are used to evaluate ice sheet
45 evolution and climate responses to orbital forcing (e.g., Liautaud et al., 2020; Raymo et al., 2006;
46 Tzedakis et al., 2017). The global "LR04" Plio-Pleistocene stack is one of the most commonly

47 used benthic $\delta^{18}\text{O}$ stacks (Lisiecki & Raymo, 2005). Given its wide use, the accuracy of LR04,
48 even in relatively minor details, has important implications for a broad range of
49 paleoceanographic applications.

50
51 Wilkens et al. (2017) identified 1.8-1.9 Ma as a period where the LR04 stack differs significantly
52 from a benthic $\delta^{18}\text{O}$ stack of five Ceara Rise cores. The Ceara Rise stack exhibits fewer glacial
53 cycles compared to LR04 during 1.8-1.9 Ma, casting doubt on how globally representative LR04
54 was during the early Pleistocene. Wilkens et al. (2017) attributed the discrepancy to LR04's
55 choice of the initial alignment target records, ODP (Ocean Discovery Program) sites 677 and 849.
56 Sites 677 and 849 use splicing to construct continuous records from adjacent drill holes, a
57 common practice for achieving complete recovery at ODP sites. Problems with splicing, Wilkens
58 et al. contended, might have made sites 677 and 849 records inaccurate.

59
60 Several recent advances provide us with an opportunity to place in a broader context the
61 discrepancy with LR04 found by Wilkens et al. (2017). First, newly developed software for
62 stacking benthic $\delta^{18}\text{O}$ records requires fewer input records and enables us to efficiently construct
63 regional stacks (Lee and Rand et al., 2023), which can reveal spatial variability that is otherwise
64 masked in global stacks (Lisiecki & Raymo, 2009; Lisiecki & Stern, 2016; Skinner & Shackleton,
65 2005; Stern & Lisiecki, 2014). We can thus assess whether the pattern seen in the Ceara Rise
66 stack is representative of regional or global changes. Second, the subsequent publication of
67 higher-resolution Atlantic records, e.g., Hodell and Channell (2016), allows an investigation into
68 the 1.8-1.9 Ma period with less ambiguity. Third, the observation of a Laurentide meltwater
69 event during the 1.8-1.9 Ma period (Shakun et al., 2016) points to a potential mechanistic
70 explanation for the Ceara Rise $\delta^{18}\text{O}$ signal identified by Wilkens et al. Here, we apply these new
71 data and techniques to demonstrate that the 1.8-1.9 Ma period stands out as an unusual instance
72 of regional divergence in Pleistocene benthic $\delta^{18}\text{O}$. We discuss the mechanisms that could have
73 caused this divergence and implications for the LR04 stack.

74 75 **Methods**

76 We construct new Pleistocene regional Atlantic and Pacific Pleistocene stacks using 209 benthic
77 $\delta^{18}\text{O}$ records, including 55 records from LR04 (Lisiecki & Raymo, 2005), 132 additional records
78 from the ProbStack (Ahn et al., 2017), and 22 recently published records identified by this study
79 (Table S1; Fig. S1-2). Many of the newly added records have relatively high resolutions,
80 resulting in a 48% increase in data points compared to the ProbStack (Figs. S1-2). Over the
81 Pleistocene, the Pacific stack includes data from 80 cores while the Atlantic stack includes data
82 from 119 cores. To evaluate the hypothesis of Wilkens et al. (2017), we also construct shorter
83 regional stacks for the Atlantic and the Pacific from 1.5 to 2.1 Ma. Between 1.8-1.9 Ma, there are
84 14 Pacific cores and 25 Atlantic cores. An Indian Ocean stack was not constructed because only
85 one record is available from the Indian Ocean during 1.8-1.9 Ma.

86
87 The new stacks are created using Bayesian Inference Gaussian Process regression and
88 Multiproxy Alignment for Continuous Stacks (BIGMACS), which is a newly developed software
89 package for probabilistically stacking ocean sediment core data and constructing multiproxy age
90 models (Lee and Rand et al., 2023). Unlike other probabilistic benthic $\delta^{18}\text{O}$ alignment software
91 (Ahn et al., 2017; Lin et al., 2014), BIGMACS can reliably construct benthic $\delta^{18}\text{O}$ stacks using a
92 smaller number of cores because it estimates a time-continuous signal using Gaussian process

93 regression (Rasmussen & Williams, 2005). This enhances our ability to create and compare
 94 benthic $\delta^{18}\text{O}$ stacks for the Atlantic and the Pacific back to the early Pleistocene (see below).
 95 Another advancement of BIGMACS is that it probabilistically integrates additional depth-age
 96 estimates provided by the user.
 97
 98 BIGMACS stack construction requires an initial alignment target, for which we used the LR04
 99 global stack (Lisiecki & Raymo, 2005). However, because the LR04 stack may not be a good
 100 representation of $\delta^{18}\text{O}$ variability from 1.8-1.9 Ma, its use as an initial alignment target could be
 101 problematic. For the 1.5-2.1 Ma stacks, we assigned additional age control points in BIGMACS
 102 for records that have sufficient resolution by visually identifying the glacial maxima associated

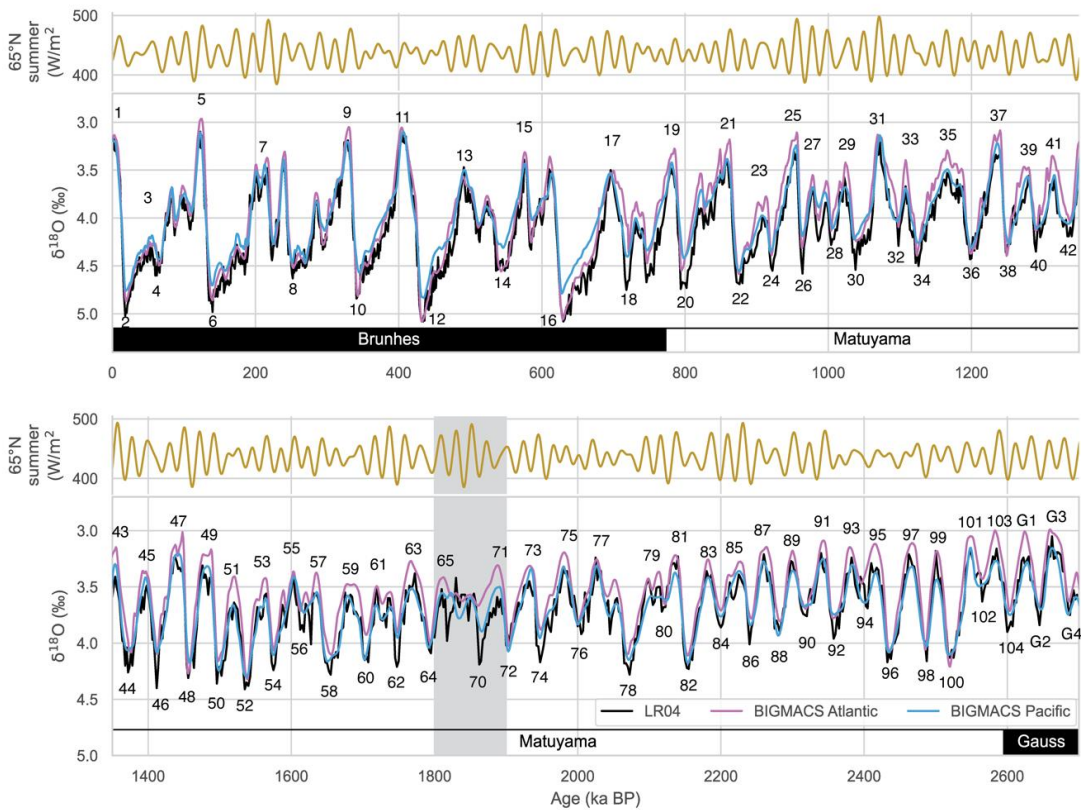


Figure 1. BIGMACS regional Pleistocene stacks for the Pacific (blue) and Atlantic (purple) without added tie points. The results presented are the stack means. Also shown is the LR04 global stack (black). The gray area is the 1.8-1.9 Ma period when the two BIGMACS regional stacks diverge. Also shown on top is the summer insolation at 65 °N. The numbers mark the Marine Isotope Stages. The black and white rectangles denote the geomagnetic chrons.

103
 104 with MIS 64 and 74 and assigning them ages based on the respective obliquity minima (1.793
 105 and 1.958 Ma). Because of the disagreement particularly between the LR04 global stack and

106 Atlantic records, we additionally identified the glacial maxima associated with MIS 68 and 70 in
107 the Atlantic records that have sufficient resolution and assigned them as “additional ages” in
108 BIGMACS based on the respective Northern Hemisphere (NH) insolation minima (1.841 and
109 1.864 Ma) with a 1-kyr standard deviation. (MIS 66 was not used because it was poorly defined
110 in most high-resolution records.) In selecting these age constraints, we are guided by the average
111 normalized sedimentation rate to ensure it is relatively steady and with no large deviations
112 between tie points (Text S1, Fig. S3). We do not propose that these age assignments are
113 necessarily appropriate corrections to the MIS ages of the LR04 stack; we merely use them to
114 ensure consistent alignments in BIGMACS where fit to the original LR04 stack is poor. The
115 discrepancies in the regional stacks between 1.8-1.9 Ma can also be seen in the full Pleistocene
116 stacks for which we did not set any additional age controls (Text S2 and Fig. 1); however, the
117 assigned age control points do affect the glacial-interglacial features of the regional stacks from
118 1.8-1.9 Ma (Fig. 2). Further details on the settings and parameters we used in BIGMACS are
119 available (Text S2).

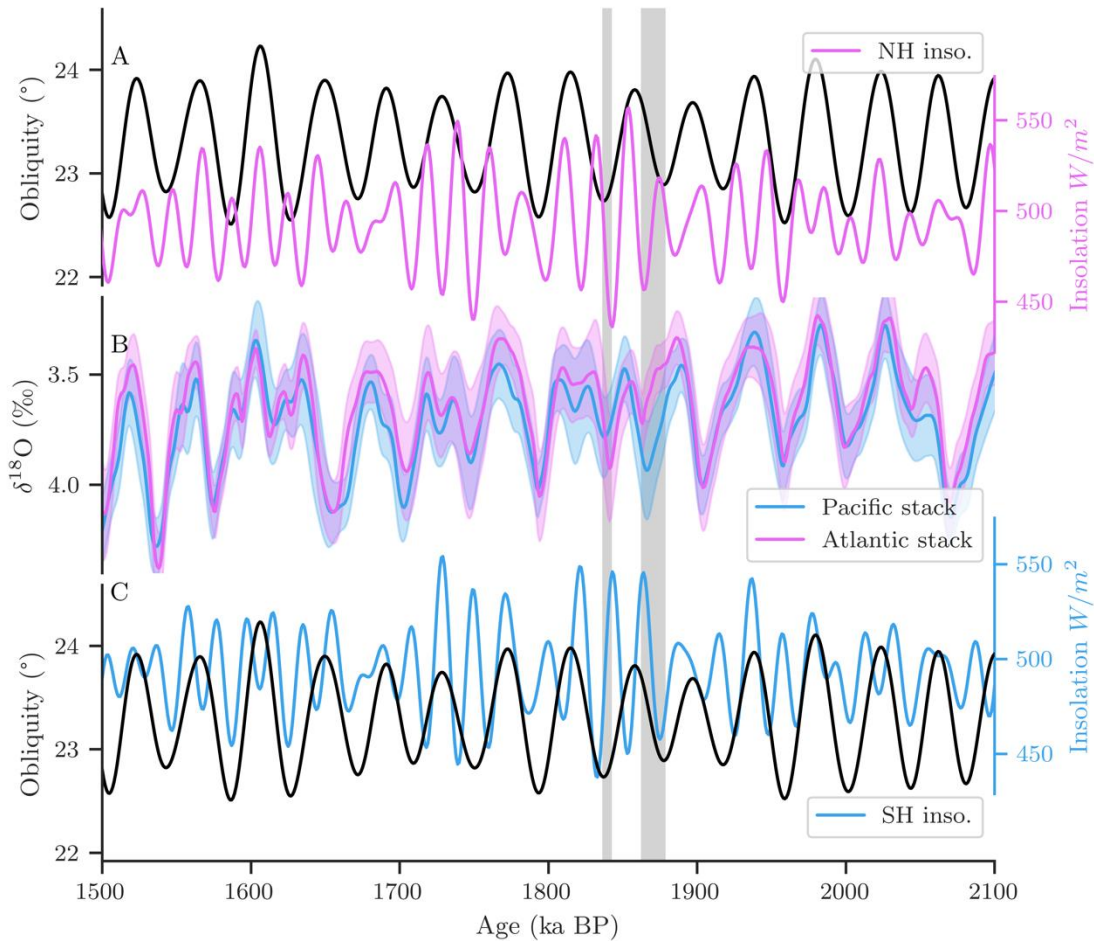


Figure 2. BIGMACS Atlantic and Pacific regional stacks compared to orbital parameters. (A) Obliquity (black) and summer insolation at 65°N (purple). The results presented are the stack means. (B) BIGMACS Atlantic (purple) and Pacific (blue) regional stacks. Shading denotes the 1 σ uncertainty of the stack $\delta^{18}\text{O}$ values. (C) Obliquity (black) and summer insolation at 65°S (blue). The vertical gray shades associate glacial periods in the regional benthic $\delta^{18}\text{O}$ stacks with the corresponding orbital parameters.

120

121 Can we detect the same Atlantic-Pacific difference in the classic LR04 stack (Lisiecki & Raymo,
 122 2005)? We separated the input records of LR04 based on ocean basins using the same $\delta^{18}\text{O}$ data
 123 on the age models used to construct the LR04 stack and binned at the same 2.5-kyr resolution
 124 used for the LR04 stack from 1.5-3 Ma. We refer to these results as the LR04 Atlantic/Pacific
 125 binned stacks.

126

127 Results

128 The new Pleistocene Atlantic and Pacific stacks, for the most part, closely follow each other
 129 except at a few places, notably during 1.8-1.9 Ma (Fig. 1). In the 1.5-2.1 Ma stacks with tie-
 130 point-guided alignments (Fig. 2), the glacial maximum at ~1.863 Ma (MIS 70) is much stronger

131 in the Pacific than the Atlantic. In comparison to other glacial maxima from 1.5-2.1 Ma, the
132 Atlantic benthic $\delta^{18}\text{O}$ response at MIS 70 more closely resembles a cold isotopic substage within
133 a long interglacial than a glacial maximum. In contrast, the Atlantic stack's glacial maximum at
134 ~ 1.841 Ma (MIS 68) is stronger than in the Pacific stack. The 1.5-2.1 Ma Atlantic stack differs
135 substantially from both LR04 and ProbStack (Ahn et al., 2017) from 1.8-1.9 Ma, more closely
136 resembling the Ceara Rise stack incorporated in CENOGRID (Wilkens et al., 2017; Westerhold
137 et al., 2020) (Fig. S4). LR04 shows two poorly resolved glacial intervals (MIS 66 and 68)
138 between two relatively normal glacial maxima (MIS 64 and 70); in contrast, the new Atlantic
139 stack has a very weak MIS 70 while MIS 68 is similar in magnitude to MIS 64 and 72. However,
140 marine isotope stages of the Pacific stack are similar to those in ProbStack from 1.8-1.9 Ma but
141 with substantially smaller 95% confidence intervals. Another Atlantic-Pacific difference appears
142 at ~ 2.05 Ma during the transition from glacial MIS 78 to interglacial MIS 77, during which the
143 Atlantic stack shows a stronger interglacial substage (similar to LR04) than the Pacific stack.
144

145 Like the regional BIGMACS stacks, the LR04 Atlantic and Pacific binned stacks differ from one
146 another between 1.8-1.9 Ma (Fig. S5). MIS 66 and 68 are absent in the LR04 Atlantic binned
147 stack, whereas the Pacific binned stack matches LR04 well. Discrepancies in the relative
148 amplitudes of MIS 68 and 70 between the Atlantic stacks produced by BIGMACS and LR04
149 binning may be caused by alignment errors during LR04 construction associated with relatively
150 low-resolution Atlantic records. The new BIGMACS Atlantic stack contains more than double
151 the $\delta^{18}\text{O}$ measurements of the LR04 Atlantic binned stack from 1.8-1.9 Ma.
152

153 **Discussion**

154 **Stratigraphic implications**

156
157 In all versions of the regional stacks we evaluated (with and without tie points), Atlantic benthic
158 $\delta^{18}\text{O}$ exhibits a different pattern of variability than the Pacific between 1.8-1.9 Ma. Differences
159 between regional stacks and the LR04 global stack at this time also provide a potential
160 explanation for previous studies, including Wilkens et al. (2021), that found discrepancies with
161 the LR04 stack between 1.8-1.9 Ma. For example, modeled ice volume differed more than
162 normal from a benthic $\delta^{18}\text{O}$ record aligned to LR04 during 1.8-1.9 Ma (Liautaud et al., 2020 and
163 Fig. 4b therein), probably because of distorted glacial cycles in the LR04 stack. A problem with
164 the LR04 stack is also suggested by a divergence of ~ 30 kyr between tuned and untuned (depth-
165 derived) age estimates for the LR04 stack from 1.8-1.9 Ma (Lisiecki, 2010 and Fig. S1 therein).
166

167 Regardless of the cause of the Atlantic-Pacific divergence, our results demonstrate that regional
168 benthic $\delta^{18}\text{O}$ stacks are preferable to global stacks for age model development by stratigraphic
169 alignment. The LR04 stack was created by performing pairwise alignment on all benthic $\delta^{18}\text{O}$
170 records to a target record. The targets were picked because of their relatively high resolution, low
171 noise, and lack of apparent hiatuses. During 1.8-1.9 Ma, LR04 used two sites, ODP 677 and 849,
172 to construct two stacks and observed that the resulting stack was largely independent of the
173 target used. However, both sites 677 and 849 are from the Pacific, which our analysis show are
174 quite dissimilar to Atlantic $\delta^{18}\text{O}$ records between 1.8-1.9 Ma. The poor fit between Atlantic
175 records and the Pacific targets likely resulted in localized alignment errors for the Atlantic
176 records.

177
178 The delicate task of choosing the right target cores for alignment is alleviated by the algorithmic
179 approaches of HMM-Stack and BIGMACS (Ahn et al., 2017; Lee and Rand et al., 2023). These
180 software packages align records to a target but iteratively update the alignment target to
181 incorporate information from all other cores, thus reducing the reliance on the user-specified
182 target. However, Atlantic and Pacific records were not analyzed separately when HMM-Stack
183 was used to construct ProbStack. The iterative approach of BIGMACS was sufficient to identify
184 a difference between the Atlantic and Pacific stacks without tie points (Fig. 1), but using the
185 LR04 stack as our initial guess for the regional stacks resulted in ambiguous alignments and
186 distortion of the glacial cycle features from 1.8-1.9 Ma. Ultimately, we bypassed this issue by
187 manually defining several tie points for glacial maxima between 1.79-1.96 Ma for the benthic
188 $\delta^{18}\text{O}$ records in which the glacial maxima could be confidently identified (Fig. S6).

189 190 **Mechanisms for generating benthic $\delta^{18}\text{O}$ gradients in the 41-kyr world**

191
192 Although benthic $\delta^{18}\text{O}$ is often considered a well-mixed proxy for global ice volume, one
193 possible explanation for the regional difference in benthic $\delta^{18}\text{O}$ from 1.8-1.9 Ma may be
194 differences in the deep water temperature or salinity of the two ocean basins. The modern global
195 ocean mixing time of oxygen isotopes is about 1500 years (Broecker & Peng, 1983; Rohling,
196 2013), which is too short to explain gradients in seawater $\delta^{18}\text{O}$ that persist on orbital timescales
197 (Morée et al., 2021). In contrast, regional variations in benthic $\delta^{18}\text{O}$ values associated with
198 differences in deep water temperature or salinity may persist over tens of thousands of years. For
199 example, regional differences observed in the amplitude of benthic $\delta^{18}\text{O}$ change during the last
200 interglacial period (MIS 5) are most easily interpreted as temperature or salinity gradients
201 between deep water masses (Lisiecki & Stern, 2016). During the 41-kyr world, the amplitude of
202 global ice volume change is smaller in magnitude such that potential regional gradients in deep
203 water temperature or salinity might constitute a larger percentage of the benthic $\delta^{18}\text{O}$ signal.

204
205 Benthic $\delta^{18}\text{O}$ values recorded for Pacific Deep Water (PDW) and North Atlantic Deep Water
206 (NADW) could differ if the temperature or salinity the two water masses exhibited sensitivity to
207 different forcings. For example, Raymo et al. (2006) asserted that the temperature/salinity of the
208 Southern Ocean likely co-varied with the changes in the Antarctic ice volume; such Southern
209 Ocean changes would also be expected to affect Antarctic Bottom Water (AABW) and PDW. At
210 the same time, the NADW temperature or salinity signal would likely have changed concurrently
211 with NH ice sheet dynamics (Marcott et al., 2011).

212
213 Circulation reconstructions for the 41-kyr world are consistent with deep water in the Atlantic
214 and Pacific responding to different hemispheric insolation forcing between 1.8-1.9 Ma. The 41-
215 kyr world Atlantic was primarily under the influence of the northern-sourced water, which filled
216 most of the mid-depth to deep Atlantic, while southern-sourced water occasionally occupied the
217 bottom depths (Cronin et al., 1996; Jakob et al., 2021; Lang et al., 2016; Zhang et al., 2013).
218 Although the 41-kyr world Pacific might have seen deep water formation in the subarctic North
219 Pacific (Burls et al., 2017; Ford et al., 2022), this northern-sourced Pacific deep water was
220 limited to depths shallower than 3000 m. Antarctic-sourced bottom water is thought to have
221 filled the deep Pacific below 3000 m (Burls et al., 2017; Ford et al., 2022), the depths from
222 which most high-resolution Pacific cores in our compilation were recovered. The only two high-

223 resolution Pacific cores in our compilation retrieved from sites shallower than 3000 m, ODP
224 1143 and 1241, display different benthic $\delta^{18}\text{O}$ patterns than the deeper cores (Figs. S6 and S8),
225 possibly due to the influence of NPDW.

226
227 We tentatively attribute the regional benthic $\delta^{18}\text{O}$ divergence to the effects of deep water
228 temperature and/or salinity because we are unable to differentiate the impacts of temperature and
229 salinity using only benthic $\delta^{18}\text{O}$. One bottom water temperature record from the Atlantic
230 suggests that deep water temperature and benthic $\delta^{18}\text{O}$ co-vary during 1.8-1.9 Ma (Sosdian &
231 Rosenthal, 2009), possibly hinting at the important influence of bottom water temperature on
232 Atlantic benthic $\delta^{18}\text{O}$ during this period. As far as we are aware, there is not a commensurate
233 Pacific deep water temperature record that can resolve glacial-interglacial cycles during 1.8-1.9
234 Ma. Such a record could shed more light on the role deep water temperature played in the
235 Atlantic-Pacific divergence in benthic $\delta^{18}\text{O}$ records.

236

237 **Antiphased Precession Effects between 1.8-1.9 Ma**

238

239 Although orbital insolation is consistently dominated by precession (Fig. 3), benthic $\delta^{18}\text{O}$ records
240 exhibit strong 41-kyr obliquity cycles during the late Pliocene/early Pleistocene. This mismatch
241 between the substantial role that precession played in modulating the NH summer insolation and
242 the apparent lack of a precessional imprint in geological records is termed the “41-kyr problem”
243 (Raymo & Nisancioglu, 2003; Watanabe et al., 2023). Many researchers have put forward
244 theories on why the 41-kyr world is dominated by obliquity. Among them, the Antiphase
245 Hypothesis has particular appeal to explain our observations (Morée et al., 2021; Raymo et al.,
246 2006). The Antiphase Hypothesis proposes that opposing responses of the northern and southern
247 hemisphere ice sheets on precessional time scales canceled each other out in the global ice
248 volume signal. For example, while cool NH summers lead to northern ice growth, coeval warm
249 Southern Hemisphere (SH) summers act to shrink the Antarctic Ice Sheet. Obliquity, which
250 exerts a symmetric effect on both hemispheres, is left as the governing cyclicality of global ice
251 volume during this period.

252

253 The Antiphase Hypothesis provides a framework to explain the Atlantic-Pacific difference in
254 benthic $\delta^{18}\text{O}$ records during 1.8-1.9 Ma (Fig. 2). While obliquity still paces the glacial-
255 interglacial cycles in global ice volume, the opposite phase of the northern and southern
256 hemisphere insolation on precession time scales could have influenced the magnitudes of glacial
257 benthic $\delta^{18}\text{O}$ change in the Atlantic and the Pacific. In particular, the 1.8-1.9 Ma time interval
258 experienced uniquely strong precession and weak obliquity relative to the rest of the 41-kyr
259 world (Fig. 3). While high-latitude summer insolation is always dominated by precession
260 (Raymo & Nisancioglu, 2003), the contrast between the strong precession and weak obliquity
261 during 1.8-1.9 Ma stands out. Other times of similar relative power of obliquity and precession
262 forcing are not directly comparable because they occur before or after the 41-kyr world, e.g., 0.9-
263 1 Ma and 3-3.1 Ma. Before the 41-kyr world, the northern hemisphere was largely ice-free
264 (Sosdian & Rosenthal, 2009). After the 41-kyr world, the Laurentide ice sheet expanded in size
265 and the glacial cycles transitioned to 100-kyr pacing (Lisiecki & Raymo, 2007). The 1.8-1.9 Ma
266 period is, thus, a unique window of time when more precession response might be expected
267 compared to the rest of the 41-kyr world.

268

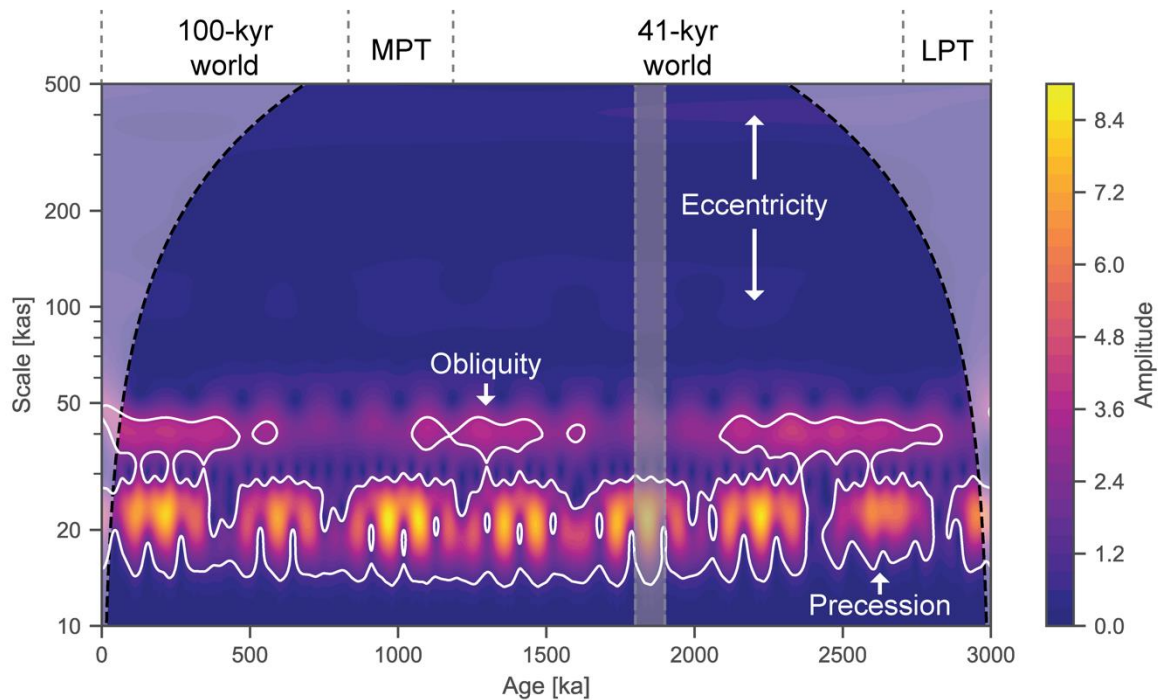


Figure 3. Wavelet spectrum of insolation at 65° N for the Plio-Pleistocene generated with Wavelet Continuous Transform using the Morlet wavelet (Torrence and Compo, 1998). The white lines delineate regions of the spectrum that are significant against a random AR(1) benchmark. The dashed lines denote the 1.8-1.9 Ma period where the Atlantic and Pacific records diverge. LPT: Late Pliocene Transition (Sosdian and Rosenthal, 2009). MPT: Mid-Pleistocene Transition. This figure was generated with Pyleoclim (Khider et al., 2022).

269
270

271 Examining the northern and southern summer insolation forcing from 1.8-1.9 Ma (Fig. 2), we
272 find that the magnitudes of the Atlantic and Pacific glacial responses are likely caused by the
273 hemispheric insolation differences during the obliquity minima. The obliquity minimum at 1.878
274 Ma coincided with a maximum in NH summer insolation and minimum SH summer insolation
275 due to the opposite hemispheric effects of precession on seasonal insolation. The Southern Ocean
276 and PDW would be expected to cool strongly during MIS 70 because SH insolation is low during
277 the obliquity minimum. In contrast, moderately high NH insolation would produce a weaker and
278 delayed glacial response for MIS 70 in northern hemisphere climate and NADW. By the time
279 NH summer insolation reaches its minimum, obliquity is relatively high and would quickly
280 reverse the NH cooling trend. Hemispheric circumstances are reversed during MIS 68 with NH
281 summer insolation low early during the obliquity minimum (amplifying NH/NADW cooling)
282 while Southern Ocean/PDW cooling is delayed by a SH insolation peak, which would initially
283 suppress SH cooling. However, because the SH insolation minimum was not as far offset from
284 the obliquity minimum during MIS 68 as the NH insolation was during MIS 70, the antiphase
285 insolation effect is weaker for MIS 68.

286

287 Notably, Atlantic $\delta^{18}\text{O}$ responses are similar for MIS 70 and MIS 56 at ~ 1.6 Ma (Fig. 2). They
288 are similarly weak glacials and both have NH precession maxima that coincide with obliquity
289 minima. The interesting difference between the two glacials is that the Pacific $\delta^{18}\text{O}$ response
290 matches the Atlantic during MIS 56, in contrast to the strong Pacific glacial maximum during
291 MIS 70. The discrepancy in Atlantic-Pacific divergence could be because MIS 70 has stronger
292 precession forcing and weaker obliquity than MIS 56. Thus, the relatively strong power of
293 precession forcing from 1.8-1.9 Ma may account for the greater regional benthic $\delta^{18}\text{O}$ difference
294 during this time compared to the rest of the 41-kyr world, leaving vestiges of precession-driven
295 regional temperature/salinity signals in the otherwise obliquity-dominated global ice volume
296 component of benthic $\delta^{18}\text{O}$.

297
298 Another potential impact of strong precession forcing during the 1.8-1.9 Ma period is a
299 Laurentide meltwater event in the Gulf of Mexico similar to or even larger in magnitude than
300 those in the late Pleistocene (Shakun et al., 2016). Alignment of the Gulf of Mexico core which
301 records this meltwater event to our Atlantic stack (Fig. S6, bottom panel) suggests that the event
302 occurred during MIS 71, immediately before the very weak glacial maximum in the Atlantic.
303 Terrestrial deposits along the Mississippi River dated to 1.8-2.0 Ma additionally substantiate the
304 size and timing of this Gulf of Mexico meltwater drainage event (Rovey II & Spoering, 2020),
305 indicating a rapid loss of Laurentide ice similar to meltwater events during the last deglaciation
306 (Barber et al., 1999; Tarasov & Peltier, 2005). As this early Pleistocene meltwater event
307 coincides with one of the weakest obliquity maxima of the 41-kyr world, it suggests sensitivity
308 of the Laurentide ice sheet to the strong precession forcing at this time. Additionally, the
309 meltwater event may have directly or indirectly contributed to the weaker Atlantic benthic $\delta^{18}\text{O}$
310 response during MIS 70. For example, the large meltwater input to the North Atlantic could have
311 slowed deep water mixing times between the Atlantic and Pacific relative to their average for the
312 41-kyr world, prolonging the Atlantic-Pacific benthic $\delta^{18}\text{O}$ contrast. The weak Atlantic benthic
313 $\delta^{18}\text{O}$ response during MIS 70 could also be accentuated by dissolution of benthic foraminiferal
314 calcite in the Atlantic if the preceding meltwater event prolonged the residence time of North
315 Atlantic Deep Water; however, dissolution is unlikely to fully account for the Atlantic-Pacific
316 discrepancy (Text S3).

317
318 Our assertion that precession, in addition to obliquity, affects the 41-kyr world glacial cycles
319 joins an array of previous studies reaching similar conclusions. An early study observed an
320 increased response to precession in benthic $\delta^{18}\text{O}$ beginning at ~ 2.5 Ma (Lisiecki & Raymo,
321 2007). Another study detected a nontrivial precession contribution to benthic $\delta^{18}\text{O}$ variability
322 from 1-3 Ma using Empirical Nonlinear Orbital Fitting (Liautaud et al., 2020). More recently,
323 precession influence during the 41-kyr world has been shown in sedimentary elemental records
324 (Sun et al., 2021), sea level (Vaucher et al., 2021), ice-rafted debris (Barker et al., 2022), and ice
325 sheet modeling (Watanabe et al., 2023). Compared to the existing evidence, our finding suggests
326 that between 1.8-1.9 Ma benthic $\delta^{18}\text{O}$ – the data originally used to demonstrate the “41-kyr
327 problem” (Raymo & Nisancioglu, 2003) – responds to precession forcing differently depending
328 on geographical locations, likely due to the different source regions of deep water masses.

329 330 **Conclusion**

331 Benthic $\delta^{18}\text{O}$ from five Ceara Rise sites was previously shown to differ from the LR04 global
332 benthic $\delta^{18}\text{O}$ stack between 1.8-1.9 Ma (Wilkens et al., 2017). Our investigation reveals that

333 discrepancy with the LR04 stack is widespread over this time interval; most Atlantic $\delta^{18}\text{O}$
334 records show a different pattern of Marine Isotope Stages than Pacific $\delta^{18}\text{O}$ records during 1.8-
335 1.9 Ma. The largest difference between the Atlantic and Pacific benthic $\delta^{18}\text{O}$ stacks occurs
336 during MIS 70 at ~ 1.878 Ma, and 1.8-1.9 Ma is the only portion of the Pleistocene for which
337 glacial cycles in the regional stacks differ substantially from LR04 (Fig. 1). The next largest
338 regional difference is an isotopic substage between MIS 77 and 78 at ~ 2.05 Ma that is
339 isotopically lighter (or warmer) in the Atlantic than the Pacific. Throughout the rest of the
340 Pleistocene, the Atlantic and Pacific regional stacks agree with LR04 and ProbStack (Fig. 1).
341

342 A re-examination of the Pacific alignment targets used in the LR04 construction process from
343 1.8-1.9 Ma explains why the LR04 stack more closely resembles the Pacific records and
344 produced misalignments of the Atlantic records. This example demonstrates why regional
345 benthic $\delta^{18}\text{O}$ stacks are preferable to global stacks for age model development by stratigraphic
346 alignment. The new stacking software BIGMACS facilitates construction of regional stacks by
347 requiring fewer records to generate a stack, but it still has some sensitivity to the choice of initial
348 alignment target. The regional stacks presented here have largely inherited the orbitally tuned
349 age model of the LR04 stack, and updated regional age models, particularly from 1.8-1.9 Ma,
350 should be developed based on analysis of the regional stacks.
351

352 We propose that the cause of the Atlantic-Pacific divergence from 1.8-1.9 Ma is hemispheric
353 sensitivity to antiphased precession forcing, specifically that Atlantic benthic $\delta^{18}\text{O}$ at this time
354 was more sensitive to NH summer insolation while deep Pacific benthic $\delta^{18}\text{O}$ was more sensitive
355 to SH summer insolation. This benthic $\delta^{18}\text{O}$ discrepancy could be caused by variations in the
356 temperature or salinity of northern- versus southern-source deep water rather than requiring
357 uneven mixing of meltwater inputs. The unusually strong precession power and weak obliquity
358 power of orbital cycles from 1.8-1.9 Ma and a contemporaneous meltwater event in the Gulf of
359 Mexico lend support to the Antiphase Hypothesis as a possible mechanism to explain spatial
360 variability in benthic $\delta^{18}\text{O}$ during this portion of the 41-kyr world. Our study joins a variety of
361 others (Barker et al., 2022; Liautaud et al., 2020; Lisiecki & Raymo, 2007; Sun et al., 2021;
362 Vaucher et al., 2021; Watanabe et al., 2023) suggesting that precession, in addition to obliquity,
363 plays a role in pacing climate signals during the 41-kyr world.
364

365 **Acknowledgements**

366 This study benefited from discussions with Devin Rand and Bethany Hobart. This research was
367 funded in part by the Heising-Simons Foundation grant number 2021–2799. Use was made of
368 computational facilities purchased with funds from the National Science Foundation (CNS-
369 1725797) and administered by the Center for Scientific Computing (CSC). The CSC is supported
370 by the California NanoSystems Institute and the Materials Research Science and Engineering
371 Center (MRSEC; NSF DMR 2308708) at UC Santa Barbara. We also acknowledge high-
372 performance computing support from Casper (doi:10.5065/D6RX99HX) provided by NCAR's
373 Computational and Information Systems Laboratory, sponsored by the National Science
374 Foundation.
375

376 **Availability Statement**

377 The BIGMACS stacking software is available at <https://github.com/eilion/BIGMACS>. The
378 compiled benthic $\delta^{18}\text{O}$ records and the resulting regional stacks will be available upon
379 publication in a Figshare repository or upon request during the review process.

380 **References**

- 381 Ahn, S., Khider, D., Lisiecki, L. E., & Lawrence, C. E. (2017). A probabilistic Pliocene–
382 Pleistocene stack of benthic $\delta^{18}\text{O}$ using a profile hidden Markov model. *Dynamics and*
383 *Statistics of the Climate System*, 2(1). <https://doi.org/10.1093/climsys/dzx002>
- 384 Barber, D. C., Dyke, A., Hillaire-Marcel, C., Jennings, A. E., Andrews, J. T., Kerwin, M. W., et
385 al. (1999). Forcing of the cold event of 8,200 years ago by catastrophic drainage of
386 Laurentide lakes. *Nature*, 400(6742), 344–348. <https://doi.org/10.1038/22504>
- 387 Barker, S., Starr, A., van der Lubbe, J., Doughty, A., Knorr, G., Conn, S., et al. (2022). Persistent
388 influence of precession on northern ice sheet variability since the early Pleistocene.
389 *Science*, 376(6596), 961–967. <https://doi.org/10.1126/science.abm4033>
- 390 Broecker, W. S., & Peng, T.-H. (1983). *Tracers in the sea*. <https://doi.org/10.1016/0016->
391 [7037\(83\)90075-3](https://doi.org/10.1016/0016-7037(83)90075-3)
- 392 Burls, N. J., Fedorov, A. V., Sigman, D. M., Jaccard, S. L., Tiedemann, R., & Haug, G. H.
393 (2017). Active Pacific meridional overturning circulation (PMOC) during the warm
394 Pliocene. *Science Advances*, 3(9), e1700156. <https://doi.org/10.1126/sciadv.1700156>
- 395 Cronin, T. M., Raymo, M. E., & Kyle, K. P. (1996). Pliocene (3.2–2.4 Ma) ostracode faunal
396 cycles and deep ocean circulation, North Atlantic Ocean. *Geology*, 24(8), 695–698.
397 [https://doi.org/10.1130/0091-7613\(1996\)024<0695:PMOFCA>2.3.CO;2](https://doi.org/10.1130/0091-7613(1996)024<0695:PMOFCA>2.3.CO;2)
- 398 Ford, H. L., Burls, N. J., Jacobs, P., Jahn, A., Caballero-Gill, R. P., Hodell, D. A., & Fedorov, A.
399 V. (2022). Sustained mid-Pliocene warmth led to deep water formation in the North
400 Pacific. *Nature Geoscience*, 15(8), 658–663. <https://doi.org/10.1038/s41561-022-00978-3>
- 401 Hodell, D. A., & Channell, J. E. T. (2016). Mode transitions in Northern Hemisphere glaciation:
402 co-evolution of millennial and orbital variability in Quaternary climate. *Climate of the*
403 *Past*, 12(9), 1805–1828. <https://doi.org/10.5194/cp-12-1805-2016>

404 Jakob, K. A., Pross, J., Link, J. M., Blaser, P., Hauge Braaten, A., & Friedrich, O. (2021). Deep-
405 ocean circulation in the North Atlantic during the Plio-Pleistocene intensification of
406 Northern Hemisphere Glaciation (~2.65–2.4 Ma). *Marine Micropaleontology*, *165*,
407 101998. <https://doi.org/10.1016/j.marmicro.2021.101998>

408 Khider, D., Emile-Geay, J., Zhu, F., James, A., Landers, J., Ratnakar, V., & Gil, Y. (2022).
409 Pyleoclim: Paleoclimate Timeseries Analysis and Visualization With Python.
410 *Paleoceanography and Paleoclimatology*, *37*(10), e2022PA004509.
411 <https://doi.org/10.1029/2022PA004509>

412 Lang, D. C., Bailey, I., Wilson, P. A., Chalk, T. B., Foster, G. L., & Gutjahr, M. (2016).
413 Incursions of southern-sourced water into the deep North Atlantic during late Pliocene
414 glacial intensification. *Nature Geoscience*, *9*(5), 375–379.
415 <https://doi.org/10.1038/ngeo2688>

416 Lee, T., Rand, D., Lisiecki, L. E., Gebbie, G., & Lawrence, C. (2023). Bayesian age models and
417 stacks: combining age inferences from radiocarbon and benthic $\delta^{18}\text{O}$ stratigraphic
418 alignment. *Climate of the Past*, *19*(10), 1993–2012. [https://doi.org/10.5194/cp-19-1993-](https://doi.org/10.5194/cp-19-1993-2023)
419 [2023](https://doi.org/10.5194/cp-19-1993-2023)

420 Liautaud, P. R., Hodell, D. A., & Huybers, P. J. (2020). Detection of significant climatic
421 precession variability in early Pleistocene glacial cycles. *Earth and Planetary Science*
422 *Letters*, *536*, 116137. <https://doi.org/10.1016/j.epsl.2020.116137>

423 Lin, L., Khider, D., Lisiecki, L. E., & Lawrence, C. E. (2014). Probabilistic sequence alignment
424 of stratigraphic records. *Paleoceanography*, *29*(10), 976–989.
425 <https://doi.org/10.1002/2014PA002713>

426 Lisiecki, L. E. (2010). Links between eccentricity forcing and the 100,000-year glacial cycle.
427 *Nature Geoscience*, 3(5), 349–352. <https://doi.org/10.1038/ngeo828>

428 Lisiecki, L. E., & Raymo, M. E. (2005). A Pliocene-Pleistocene stack of 57 globally distributed
429 benthic $\delta^{18}\text{O}$ records. *Paleoceanography*, 20(1), 1–17.
430 <https://doi.org/10.1029/2004PA001071>

431 Lisiecki, L. E., & Raymo, M. E. (2007). Plio–Pleistocene climate evolution: trends and
432 transitions in glacial cycle dynamics. *Quaternary Science Reviews*, 26(1), 56–69.
433 <https://doi.org/10.1016/j.quascirev.2006.09.005>

434 Lisiecki, L. E., & Raymo, M. E. (2009). Diachronous benthic $\delta^{18}\text{O}$ responses during late
435 Pleistocene terminations. *Paleoceanography*, 24(3).
436 <https://doi.org/10.1029/2009PA001732>

437 Lisiecki, L. E., & Stern, J. V. (2016). Regional and global benthic $\delta^{18}\text{O}$ stacks for the last glacial
438 cycle. *Paleoceanography*, 31(10), 1368–1394. <https://doi.org/10.1002/2016PA003002>

439 Marcott, S. A., Clark, P. U., Padman, L., Klinkhammer, G. P., Springer, S. R., Liu, Z., et al.
440 (2011). Ice-shelf collapse from subsurface warming as a trigger for Heinrich events.
441 *Proceedings of the National Academy of Sciences*, 108(33), 13415–13419.
442 <https://doi.org/10.1073/pnas.1104772108>

443 Martinson, D. G., Pisias, N. G., Hays, J. D., Imbrie, J., Moore, T. C., & Shackleton, N. J. (1987).
444 Age Dating and the Orbital Theory of the Ice Ages: Development of a High-Resolution 0
445 to 300,000-Year Chronostratigraphy. *Quaternary Research*, 27(1), 1–29.
446 [https://doi.org/10.1016/0033-5894\(87\)90046-9](https://doi.org/10.1016/0033-5894(87)90046-9)

447 Morée, A. L., Sun, T., Bretones, A., Straume, E. O., Nisancioglu, K., & Gebbie, G. (2021).
448 Cancellation of the Precessional Cycle in $\delta^{18}\text{O}$ Records During the Early Pleistocene.

449 *Geophysical Research Letters*, 48(3), e2020GL090035.
450 <https://doi.org/10.1029/2020GL090035>

451 Rasmussen, C. E., & Williams, C. K. I. (2005). *Gaussian Processes for Machine Learning*.
452 Cambridge: MIT Press.

453 Raymo, M. E., & Nisancioglu, K. H. (2003). The 41 kyr world: Milankovitch's other unsolved
454 mystery. *Paleoceanography*, 18(1). <https://doi.org/10.1029/2002PA000791>

455 Raymo, M. E., Lisiecki, L. E., & Nisancioglu, K. H. (2006). Plio-Pleistocene Ice Volume,
456 Antarctic Climate, and the Global $\delta^{18}\text{O}$ Record. *Science*, 313(5786), 492–495.
457 <https://doi.org/10.1126/science.1123296>

458 Rohling, E. J. (2013). Oxygen isotope composition of seawater. In *The Encyclopedia of*
459 *Quaternary Science* (Vol. 2, pp. 915–922). Amsterdam: Elsevier.

460 Rovey II, C. W., & Spoering, G. (2020). Age and provenance of upland gravels in Missouri,
461 USA, and their relationship to Early Pleistocene glaciation. *Boreas*, 49(2), 333–349.
462 <https://doi.org/10.1111/bor.12429>

463 Shakun, J. D., Raymo, M. E., & Lea, D. W. (2016). An early Pleistocene Mg/Ca- $\delta^{18}\text{O}$ record
464 from the Gulf of Mexico: Evaluating ice sheet size and pacing in the 41-kyr world.
465 *Paleoceanography*, 31(7), 1011–1027. <https://doi.org/10.1002/2016PA002956>

466 Skinner, L. C., & Shackleton, N. J. (2005). An Atlantic lead over Pacific deep-water change
467 across Termination I: implications for the application of the marine isotope stage
468 stratigraphy. *Quaternary Science Reviews*, 24(5), 571–580.
469 <https://doi.org/10.1016/j.quascirev.2004.11.008>

470 Sosdian, S., & Rosenthal, Y. (2009). Deep-Sea Temperature and Ice Volume Changes Across the
471 Pliocene-Pleistocene Climate Transitions. *Science*, 325(5938), 306–310.
472 <https://doi.org/10.1126/science.1169938>

473 Stern, J. V., & Lisiecki, L. E. (2014). Termination 1 timing in radiocarbon-dated regional benthic
474 $\delta^{18}\text{O}$ stacks: Regional benthic $\delta^{18}\text{O}$ stacks. *Paleoceanography*, 29(12), 1127–1142.
475 <https://doi.org/10.1002/2014PA002700>

476 Sun, Y., McManus, J. F., Clemens, S. C., Zhang, X., Vogel, H., Hodell, D. A., et al. (2021).
477 Persistent orbital influence on millennial climate variability through the Pleistocene.
478 *Nature Geoscience*, 1–7. <https://doi.org/10.1038/s41561-021-00794-1>

479 Tarasov, L., & Peltier, W. R. (2005). Arctic freshwater forcing of the Younger Dryas cold
480 reversal. *Nature*, 435(7042), 662–665. <https://doi.org/10.1038/nature03617>

481 Torrence, C., & Compo, G. P. (1998). A practical guide to wavelet analysis. *Bull. Am. Meteor.*
482 *Soc.*, 79(1), 61–78. [https://doi.org/10.1175/1520-](https://doi.org/10.1175/1520-0477(1998)079<0061:APGTWA>2.0.CO;2)
483 [0477\(1998\)079<0061:APGTWA>2.0.CO;2](https://doi.org/10.1175/1520-0477(1998)079<0061:APGTWA>2.0.CO;2)

484 Tzedakis, P. C., Crucifix, M., Mitsui, T., & Wolff, E. W. (2017). A simple rule to determine
485 which insolation cycles lead to interglacials. *Nature*, 542(7642), 427–432.
486 <https://doi.org/10.1038/nature21364>

487 Vaucher, R., Dashtgard, S. E., Horng, C.-S., Zeeden, C., Dillinger, A., Pan, Y.-Y., et al. (2021).
488 Insolation-paced sea level and sediment flux during the early Pleistocene in Southeast
489 Asia. *Scientific Reports*, 11(1), 16707. <https://doi.org/10.1038/s41598-021-96372-x>

490 Watanabe, Y., Abe-Ouchi, A., Saito, F., Kino, K., O’ishi, R., Ito, T., et al. (2023). Astronomical
491 forcing shaped the timing of early Pleistocene glacial cycles. *Communications Earth &*
492 *Environment*, 4(1), 1–11. <https://doi.org/10.1038/s43247-023-00765-x>

493 Westerhold, T., Marwan, N., Drury, A. J., Liebrand, D., Agnini, C., Anagnostou, E., et al. (2020).
494 An astronomically dated record of Earth's climate and its predictability over the last 66
495 million years. *Science*, 369(6509), 1383–1387. <https://doi.org/10.1126/science.aba6853>
496 Wilkens, R. H., Westerhold, T., Drury, A. J., Lyle, M., Gorgas, T., & Tian, J. (2017). Revisiting
497 the Ceara Rise, equatorial Atlantic Ocean: isotope stratigraphy of ODP Leg 154 from 0 to
498 5 Ma. *Climate of the Past*, 13(7), 779–793. <https://doi.org/10.5194/cp-13-779-2017>
499 Zhang, Z.-S., Nisancioglu, K. H., Chandler, M. A., Haywood, A. M., Otto-Bliesner, B. L.,
500 Ramstein, G., et al. (2013). Mid-pliocene Atlantic Meridional Overturning Circulation
501 not unlike modern. *Climate of the Past*, 9(4), 1495–1504. [https://doi.org/10.5194/cp-9-](https://doi.org/10.5194/cp-9-1495-2013)
502 1495-2013
503